Water Transport in Cellular Tissues During Thermal Processing

Amit Halder, Ashim K. Datta, and Roger M. Spanswick
Dept. of Biological and Environmental Engineering, Cornell University, Ithaca, NY 14853

DOI 10.1002/aic.12465
Published online December 3, 2010 in Wiley Online Library (wileyonlinelibrary.com).

Accurate modeling of water transport in food materials requires knowledge of how transport properties depend on the material structure. Water transport in a cellular tissue depends on its pathway (intracellular versus extracellular), which in turn depends on temperature. Using a combination of permeability measurement, pore-size distribution analysis and bioimpedance analysis, it is shown that water in a cellular tissue (e.g., potatoes) is mostly intracellular at lower temperatures at which cell membranes are intact. During drying at high-temperatures, cell membranes in potatoes are damaged, and the moisture transport pathway is primarily extracellular (through intercellular spaces and the lacunae created by the killed cells), with a much lower resistance to water transport. The difference in moisture diffusivity in potatoes for the two pathways has been estimated to be three orders of magnitude. Therefore, transport properties measured or predicted at low temperatures cannot be used for high temperatures because they correspond to different moisture migration pathways. © 2010 American Institute of Chemical Engineers *AIChE J,* 57: 2574–2588, 2011
Keywords: food, pores, bioimpedance, extracellular, intracellular, permeability

Introduction

For accurate prediction of temperature and moisture content in cellular tissues during thermal processing, it is of utmost importance to understand the different pathways that water can take during the process. The resistance to moisture migration offered by different pathways depends on the structure and composition of the tissue. Cellular foods like fruits, vegetables, and meat have complex structures and, depending on the extent of dehydration, water is found as liquid water in the pores or inside the cells. The resistance faced by liquid water in the pores is different from that faced by water inside the cells. A predictive model to simulate drying or other water removal processes in cellular foods generally uses an effective diffusivity as a function of moisture content to describe the moisture migration.[1,2] Such an effective diffusivity is an average of all the resistive pathways and is completely empirical, specific to a process and food material. But for the purpose of modeling drying processes, effective diffusivities should be based on the properties of cellular structures in addition to the moisture content of the tissue.[3,4] In more complex models of frying and drying processes,[5–7] where various transport modes of different phases of water are considered, the availability of transport properties is limited, thus reducing the usefulness of such models. It therefore becomes critical to understand how transport properties relate to the structure of materials and how they change as materials transform during the process.

The outline of this article is as follows: The literature review is followed by the objectives of the article. The theories behind capillary pressure, pore-size distribution, and bioelectrical impedance analysis (BIA) are discussed, followed by the experimental setups used. Finally, the experimental results are discussed, leading to identification of moisture migration pathways and explanation of relationship between moisture diffusivity and the structure of a cellular food material.

Correspondence concerning this article should be addressed to A. K. Datta at ah333@cornell.edu.

Literature review

To reach our goal of understanding water transport in a cellular tissue, we can start by considering the tissue as a porous medium and look into how cellular structure affects such transport. The capillary pressure and permeability measurement experiments help us to understand the porous medium. As will be shown later, it is also important to know what fraction of water is inside the cell. For this, we will use BIA.

Capillary Pressure, Permeability, and Pore-size Distribution Measurement. Capillary pressure has been routinely measured for soil structures in the field of soil science and hydrology[8–10] and for rocks in petroleum engineering.[11–13] The most common method for measuring capillary pressure is using the pressure plate technique, in which external pressure is applied to force water out of a saturated sample. Another common technique for measuring capillary pressure, in the case of rocks, is the centrifuge technique, in which water is forced out of the saturated sample by centrifugal force.[13] These experimental methods work well for rigid, noncellular and homogenous materials but need major modifications for measurements in soft and cellular tissues due to their nonhomogeneity and deformation under high pressures. Capillary pressure in green softwood was measured using the centrifuge technique.[14] Due to the lack of such data for food materials, the data for softwood has been extensively used in modeling of water transport in potatoes during frying.[6] This approach is based on the assumption that the structure of potato tubers and softwood are similar and therefore their capillary pressure should also be similar. There is no measured capillary pressure data whatsoever as we move away from wood and potato tissue into other biomaterials. Therefore, there is an acute need to develop an experimental procedure for measuring capillary pressure in food materials to facilitate the modeling of water transport during drying processes.

Permeability can be used to estimate resistance to flow offered by a pathway. Unlike capillary pressure data, there are some permeability data available for potatoes[15] and ground beef.[16] The permeability of water was measured by forcing water through the material and recording the resistance based on the flow rate coming out of the other end of the sample. Since the tissues are nonhomogenous and there is a huge difference between the largest and the smallest pores, there is significant variation in the permeabilities through these pores. The afore mentioned experiments give the permeability of the least resistant pathway or the largest pores. Therefore, to get the proper estimate of permeability, we must know the pore-size distribution of the food material.

Several studies have estimated porosity (volume of air to total volume) using gas pycnometry in the case of chicken[17] and mercury porosimetry for chicken meat,[18] but the pore-size distribution is still largely unavailable for most food materials. Quantitative characterization of porous media, as shown in breads,[19] has been rare for other products. The relationship of pore-size distribution to transport properties is also not available.

Bioelectrical Impedance Analysis. BIA gives the fraction of the water in a tissue that is intracellular. BIA measures the opposition of a tissue to an applied low-strength alternating current and, based on the measured impedance to an electrical current, estimates of intracellular water (ICW) content are made. A tissue is an imperfect conductor of electrical current. The concept of using electrical resistance or impedance to assess physiological aspects of the body dates back over 100 years, but the period of intense research in BIA started in 1985,[20] when it was demonstrated that this technology could be used to detect various immune diseases in humans. Since then, BIA has been used extensively to estimate the physiological state of various biological tissues because of its simplicity and because it can be done *in situ* without cutting or crushing. The first successful validation of measurement of extracellular and ICW inside animal tissues using BIA was reported 1992.[21] Now, measurement of intracellular and extracellular water in live animals using BIA is routine for detecting immunological diseases.

In the case of plant tissues (e.g., fruits, vegetables, roots, leaves, etc.), BIA has been used extensively in physiological investigation such as injury due to freeze-thaw cycles in potato tubers and carrot roots[22] and to estimate the extent of bruising in apples.[23] The electrical impedance of ripe and unripe nectarine fruits were compared to develop a fruit maturity index.[24] The relationship between the electrical and rheological properties of potato tuber tissue was also shown using BIA.[25] The impedance analysis was also used to study the effect of drying and freezing-thawing treatments on eggplants.[26] In all these studies, qualitative assessment of rheological properties was based on the measured impedance. Neither the estimate of ICW content nor any information regarding transport of water inside the cellular tissue was available.

Other techniques The water movement in carrots during drying and freezing was studied using an NMR technique,[27,28] which showed that drying (at 293 K) removes water from vacuolar compartment, causing cell shrinkage and concentration of dissolved solutes. The mentioned studies did not include the effect of temperature on overall diffusivity of water inside the carrot. Temperature plays a large role in moisture migration pathway, as will be shown later in this study. Similar studies for potatoes at subzero temperatures using NMR technique were done by.[29] The details of mechanisms and prevention of plant tissue collapse during dehydration at temperatures below 50°C were covered by.[30] Three pathways of water migration were discussed: intercellular spaces, wall-to-wall, and cell-to-cell. The resistances of each pathway to transport properties were not studied; hence quantification of water diffusivity using the study is not possible. Further, the above mentioned studies ignored how the cell structure influences moisture diffusivity at high temperatures, when cell membrane ruptures.

Objectives The objectives of this present study were: (1) to quantify the amount of water present in the capillaries and cells of two tissues (potato and eggplant) at different temperatures; (2) to establish different pathways of moisture transport in a cellular tissue under different processing conditions; (3) to discuss the implications of these microstructural aspects on water transport in such tissues.

Theory Behind the Measurements

Capillary pressure

Capillary pressure is the difference in pressure across the interface between two immiscible fluids, a nonwetting fluid

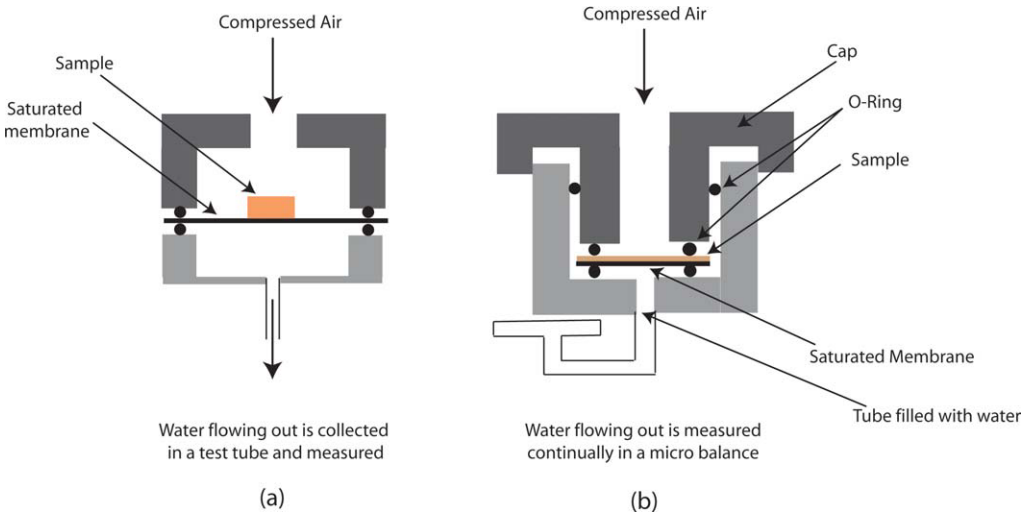

Figure 1. Schematic of the experimental setup for capillary pressure measurement.

(a) Pressure plate experiment; (b) Liquid extrusion porosimeter in Porous Materials (Ithaca, NY). [Color figure can be viewed in the online issue, which is available at wileyonlinelibrary.com.]

and a wetting fluid. When the wetting fluid is liquid water and the nonwetting fluid is air, the capillary pressure, p_{cap}, is given by

$$p_{cap} = p_a - p_w \tag{1}$$

where p_a is the air pressure and p_w is the liquid water pressure. In the case of food materials (e.g., potato, meat, etc.), what is referred to as the capillary pressure is essentially the lumped effect of surface tension, immiscibility, the presence of microscopic scale fluid–fluid interfaces, fluid viscosity, the wettability of solid surfaces, grain size distribution, microscale and macroscale heterogeneities, solid matrix deformation, and fluid composition.[31] Although processes determining the capillary pressure of water are extremely complicated, the main theoretical and practical approach currently in use for characterizing this is an empirical relationship between capillary pressure and moisture content.

Experiments conducted to calculate capillary pressure as a function of moisture content assume that all the liquid water is present in the capillaries and that it flows as long as the applied gas pressure (p_a) exceeds the capillary pressure (p_{cap}). As soon as the applied gas pressure is equal to the capillary pressure of the food material at that moisture content, the liquid water stops flowing and capillary pressure is determined from the applied gas pressure. This pressure is then related to the moisture content of the material at that point. By extending this to a number of applied pressures, a capillary pressure curve, which relates capillary pressure to moisture content, is generated.

Pressure Plate Experiment. The simplest way to force water through a porous medium is to run a pressure plate experiment.[32] The schematic of the experimental set-up is shown in Figure 1. The potato slice is placed on a saturated porous polycarbonate membrane of pore-sizes of 0.1 μm (Sterlitech Corporation, Kent, WA) in the pressure chamber. The air pressure is applied from the top. If the base of the potato slice is in good contact with the porous membrane then the liquid water in the potato slice is in continuum with the liquid water in the polycarbonate membrane. In that case, the bottom surface of the potato slice is at atmospheric pressure and there is a pressure difference between the top and bottom surfaces (equal to the magnitude of the applied gas pressure). The largest pore-size of the polycarbonate membrane is smaller than the smallest pore-size of the potato slice, so the air cannot push out water from the polycarbonate membrane before it pushes it from the potato slice. When water is pushed out of the potato slice, it replaces the water in the polycarbonate membrane which flows out into a receiver where its volume is measured.

Liquid Extrusion Porosimetry. A Liquid Extrusion Porosimeter (Porous Materials, Ithaca, NY) was used to measure the capillary pressure of the potato sample at different moisture contents. Unlike the pressure plate experiment, the pressure was raised every hour in this equipment. The maximum pressure that can be applied using this equipment is 0.7 MPa and the pressure step size used was 0.025 MPa. The amount of water drained from the potato is collected in a microbalance (0.001 g accuracy) and measured at regular intervals. The initial moisture content of the potato slice is known, so its transient moisture content is calculated from the measured drained water.

Largest Pore-Size and Pore-Size Distribution

Largest pore-size A pore-size distribution experiment gives the fraction of void volume that is occupied by different pore-sizes. The schematic of the pore-size distribution experimental setup is shown in Figure 2. The pores of the sample are assumed to be filled with water initially. Air pressure on the top surface of the sample is slowly increased so as to displace the liquid from the pores and thereby increase gas flow through the sample at the other end. The gas can displace the liquid from the pores only when the applied pressure exceeds the capillary pressure on the liquid. The differential pressure, p_{cap}, required for displacement of liquid water in a cylindrical pore is given by[33]

$$p_{cap} = 4\frac{\gamma \cos\ \theta}{d} \tag{2}$$

where γ is the surface tension of liquid water, d is the diameter of the pore and θ is the contact angle between liquid water and the surface. The pressure required to empty a pore is smallest for the largest pore (also known as the bubble point diameter) and can be estimated from Eq. 2.

Pore-size Distribution. To calculate the pore-size distribution, flow rates through wet and dry samples are determined. A wet sample is one that is initially saturated with water and, during the experiment, the water is pushed out of the sample by pressurized air. A dry sample is one that is completely dry and the pore channels are filled with air. Therefore, a wet curve (flow rate versus time for a wet sample) provides the flow rate through all the open pores at any given pressure, while a dry curve provides flow rate through all the pores (since all pores are open).

Assuming viscous flow, at a given temperature, the flow rate, F, through a porous channel is given by the product of velocity (from the Poiseuille equation) and area, shown as

$$\begin{aligned} F &= \text{area} \times \text{velocity} \\ &= \frac{\pi d^2}{4} \times \frac{d^2}{32\mu}\frac{dp}{dx} \\ &= \frac{\pi d^2}{4} \times \frac{d^2}{32\mu}\frac{p}{L} \end{aligned} \tag{3}$$

Therefore, the flow rate through N number of pores can be written as[34]

$$F = \frac{\pi}{128\mu L}\sum_{i=1}^{N} n_i d_i^4 \times p = g(d,N) \times f(p) \tag{4}$$

So, flow rate through a porous medium is a function of pressure and the pore characteristics of the sample (e.g., the diameter of the pores, d, and the number of pores, N). For viscous flow, the pressure variable is separable from the other variables and can be expressed as a product of two functions, $f(p)$ and $g(d,N)$, as shown in Eq. 4.

Therefore, the ratio of flow rates through a wet and dry sample at the same applied pressure is given by

$$[F_{\text{wet},p}/F_{\text{dry},p}] = [f(p) \times g(d,N)]_{\text{wet},p}/[f(p) \times g(d,N)]_{\text{dry},p} \tag{5}$$

The function $f(p)$ is the same for wet and dry samples and therefore the ratio of flow rates is a function of pore structure only and is given by

$$[F_{\text{wet},p}/F_{\text{dry},p}] = [g(d,N)]_{\text{wet},p}/[g(d,N)]_{\text{dry},p} \tag{6}$$

Therefore, the fraction of flow through pores with diameters between D_j and D_{j+1} is

$$\Delta F = [F_{\text{wet},p}/F_{\text{dry},p}]_{j+1} - [F_{\text{wet},p}/F_{\text{dry},p}]_j \tag{7}$$

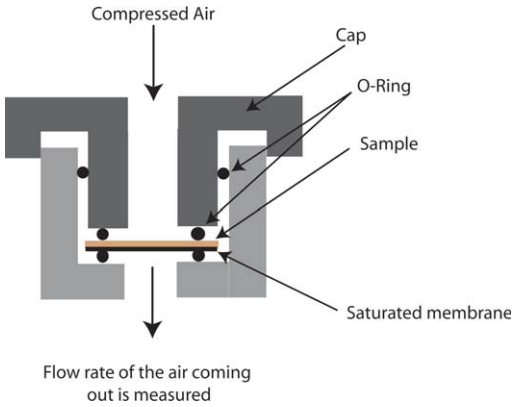

Figure 2. Schematic of the experimental setup for pore-size distribution measurement.

[Color figure can be viewed in the online issue, which is available at wileyonlinelibrary.com.]

The fraction of flow through a diameter range is equal to the fraction of pore volume in that diameter range, thus providing the pore-size distribution.

Bioelectrical impedance analysis

BIA is performed to determine the fraction of water in a tissue that is intracellular. The technology is based on the principle that electricity is conducted through a tissue by electrolyte-containing fluids and will take the path of least resistance. The simplified equivalent circuit for current flow through a tissue proposed by Zhang et al.[22] is shown in Figure 3. The total impedance, Z, can be broken down into two parts: (1) the real part, known as resistance; (2) the complex part, known as reactance. The electrical current inside the tissue experiences opposition from (1) the fluids in the tissue (extracellular and intracellular fluids); (2) the cell membrane, which has a high-resistance but acts as a capacitor (storing up electrical charge for a given electrical potential). In Figure 3, the resistance due to extracellular fluid is shown as R_e and that due to intracellular fluid (in the cytoplasm) as R_i; the impedance due to cell membrane capacitance is given as

$$Z_c = \frac{1}{j\omega C} \tag{8}$$

where Z_c is the impedance due to cell membrane capacitance, $\omega = 2\pi f$, with f being the frequency of the signal, and C is the capacitance of the cell membrane. Therefore, the total impedance of the electrical circuit is

$$Z = \frac{R_e\left(R_i + \frac{1}{j\omega C}\right)}{R_e + R_i + \frac{1}{j\omega C}} \tag{9}$$

Bioelectrical Impedance at Low Frequencies. As shown in Figure 4, at low frequencies the current applied to the tissue will travel predominantly through the extracellular fluid and only a portion of the applied current will be opposed by the cell membranes of the tissues. This is because, at low frequencies, cell membranes have high electrical resistance

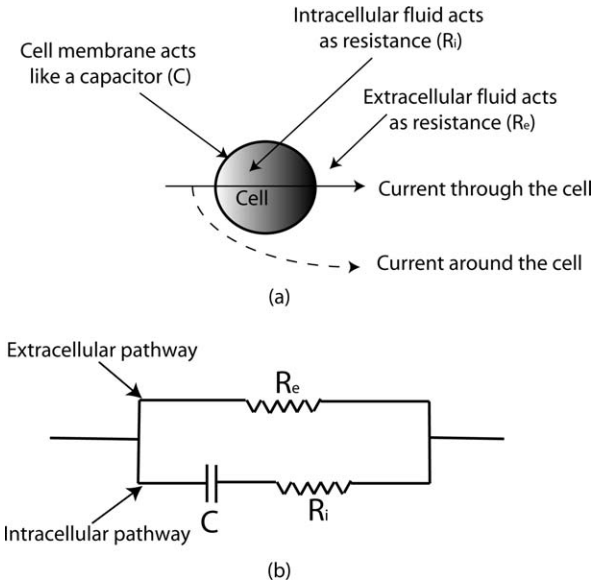

Figure 3. (a) Schematic of a cell with extracellular fluid and two pathways that a current can take (through the cell and around the cell) is shown; (b) the equivalent circuit for current through cell and extracellular fluid is shown.

This is a parallel circuit as the current can go either through the extracellular fluid or through the cell (cell membrane and intracellular fluid). The resistance of the plasma membrane, which is in parallel with the membrane capacitance, is ignored due to its relatively high value.

because the RC time constant of the cells is small. The potential gradients across the cell membranes will closely follow the external potential gradient and therefore the magnitude of the current into the cell capacitor will be small. A major part of the current goes through the extracellular compartment. R_0 is the resistance measured at zero frequency (e.g., a direct current). It is the best theoretical value of impedance of the extracellular space as almost all the current travels through this space at zero frequency.

Bioelectrical Impedance at High Frequencies. As the frequency increases, the impedance of the membrane (a capacitor) decreases, allowing more current to flow into the intracellular compartments. Because of the change in polarity due to the AC current, the cell membrane charges and discharges at the rate of the frequency. At higher frequencies, the rate of charge and discharge becomes such that the impedance due to the capacitor diminishes to insignificant proportions, and the current flows through both the extracellular and intracellular compartments in proportions that depend on their relative conductivities and volumes.[35] Thus, $R_{\inf}$ is the impedance measured at infinite frequency and is the best theoretical value of impedance due to the extracellular and intracellular fluid. Note that the infinite frequency current will not be affected by interaction with the cell membranes and that it will pass directly through the cell membranes. Hence, at this frequency the reactance component of the impedance vector is zero. In this way the impedance at $R_{\inf}$ is the impedance due to the total tissue water (intracellular and extracellular) and is given by

$$R_{\inf} = \frac{R_i R_e}{R_i + R_e} \tag{10}$$

Cole–Cole Plot. The impedance of the equivalent circuit (shown in Figure 3) at an angular frequency, ω, can be rewritten in terms of R_0 and $R_{\inf}$ as

$$\begin{aligned} Z &= R + jX \\ &= R_{\inf} + \frac{R_0 - R_{\inf}}{1 + j\omega C} \\ &= \left(R_{\inf} + \frac{R_0 - R_{\inf}}{1 + \omega^2 C^2}\right) + j\omega C\left(\frac{R_{\inf} - R_0}{1 + \omega^2 C^2}\right) \end{aligned} \tag{11}$$

A plot of reactance (X) versus resistance (R) of a tissue for various frequencies, known as a Cole–Cole plot and shown in Figure 5, gives a semicircle. The semicircular nature of the plot allows the determination of $R_{\inf}$ (a theoretical value) that cannot be measured directly. In practice, resistance (R) and reactance (X) are measured for a number of frequencies (between 5 kHz and 1 MHz) and the Cole–Cole plot is constructed and extrapolated at the ends (to touch the R-axis) to yield $R_{\inf}$ and R_0.

Ratio of ICW to Extracellular Water. The ratio of volume (V_{ICW}) to extracellular water volume (V_{ECW}) was predicted from the modeled R_0 and $R_{\inf}$ using equations formulated from theory[36] that describes the effect that a concentration of nonconductive material has on the apparent resistivity of the surrounding conductive fluid. The ratio is determined by the following equation[37]

$$\left(1 + \frac{V_{\mathrm{ICW}}}{V_{\mathrm{ECW}}}\right)^{5/2} = \frac{R_e + R_i}{R_i}\left(1 + \kappa\frac{V_{\mathrm{ICW}}}{V_{\mathrm{ECW}}}\right) \tag{12}$$

where

$$\kappa = \frac{\beta_{\mathrm{ICW}}}{\beta_{\mathrm{ECW}}} \tag{13}$$

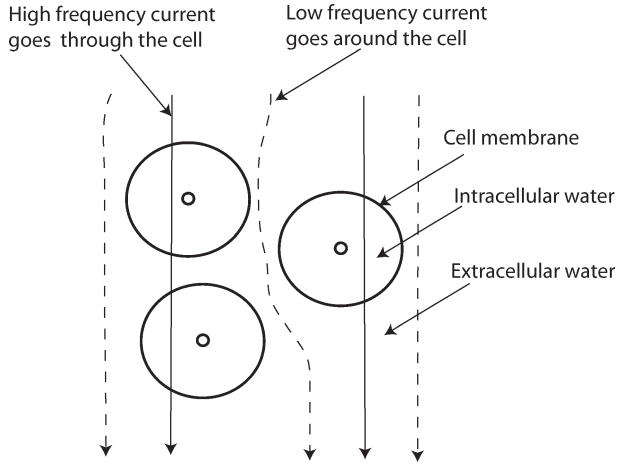

Figure 4. The responses of different frequency signals in a biological tissue are shown.

A high frequency signal can go through both the cell membrane and intracellular fluid. The low frequency signal cannot penetrate the cell membrane and therefore goes around the cell.

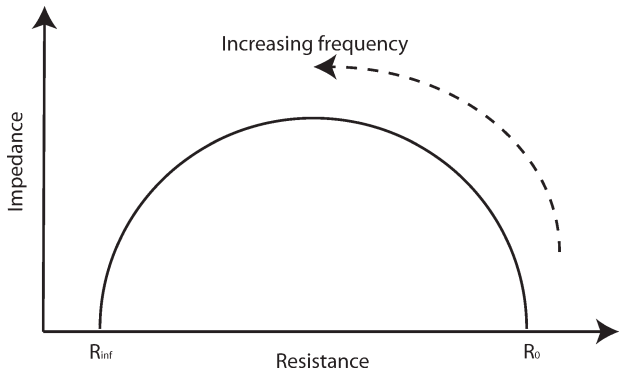

Figure 5. A Cole–Cole plot.

In practice, the resistance (R) and reactance (X) is measured for a number of frequencies (between 5 kHz and 1 MHz) and Cole–Cole plot is constructed. The ends are then extrapolated to touch the R-axis to get R_{inf} and R_0.

Equation 12 can be written in terms of R_0 and R_{inf}, using Eq. 10 and the assumption of $R_0 = R_e$, as

$$\left(1+\frac{V_{ICW}}{V_{ECW}}\right)^{5/2} = \frac{R_0}{R_{inf}}\left(1+\kappa\frac{V_{ICW}}{V_{ECW}}\right) \tag{14}$$

The parameter κ is the ratio of electrical resistivity in intracellular fluid to electrical resistivity in extracellular fluid, and has been determined for animal cells to be between 3.2 and 3.71.[37] For higher plant cells, it is not possible to measure this parameter. For animal cells it was determined that conductivity in extracellular fluid is always more than that in the intracellular fluid. In plant cell walls, there are Donnan free spaces that contain a high concentration of negative charges that are associated with mobile cations,[38] thereby conferring a high electrical conductance on the extracellular region. Therefore, we use a conservative value of κ equal to 3.2. This will give the lowest estimate of ICW volume.

Materials and Methods

Capillary pressure measurements

As will be discussed later, pressure driven flow was difficult to achieve, and consequently two separate experimental setups were tried to measure the capillary pressure of a potato sample (Russet white Idaho type) as the moisture content changes.

Setup 1: Classical Pressure Plate Experiment. Cylindrical potato samples (diameter 3 cm and thickness 2 cm) were placed in the pressure chamber (as shown in Figure 1a) at an applied pressure (0.1 MPa; 0.3 MPa; 0.5 MPa and 1.5 MPa) for 5 days and were allowed to come to equilibrium. After 5 days, the sample was taken out of the chamber and its weight was measured (the difference between the initial and final weight of the potato slice should be equal to the weight of water collected during the experiment). The relative humidity inside the chamber was at 100% (e.g., humidity was maintained by placing four beakers filled with water inside the chamber). Each time, a sample was also placed outside the chamber at 60% RH and atmospheric pressure during the course of the experiment to estimate moisture loss that would happen without applied pressure, due to evaporation. This gave the amount of water lost due to difference in relative humidity only.

Setup 2: Liquid Extrusion Porosimetry Experiment. Cylindrical potato samples (diameter 3 cm and thickness 2 cm) were placed in the pressure chamber (as shown in Figure 1b). The pressure in the chamber was increased by 0.025 MPa every hour until it reached 0.7 MPa (the maximum for the equipment). The relative humidity inside the chamber was 100%. Each time, a sample was also placed outside the chamber at 60% RH and atmospheric pressure during the course of the experiment, as explained in the previous paragraph.

Pore-size distribution measurements

Five samples of potato tissue (diameter 3 cm and thickness 2 cm) were analyzed for pore-size distribution. Each sample was placed in the pressure chamber (as shown in Figure 2) and the applied pressure was slowly increased from 0.0 to 0.7 MPa in 4 hours. The air flow sensor at the other end recorded the total air flowing out of the potato sample during the course of the experiment. At the end of the experiment, the air flow rate was plotted against the applied pressure for the wet and dry samples (a dry sample is the slice at the end of the pore-size experiment from which the water has been forced out) and the pore-size distribution was estimated as explained above in the theory section.

Bioelectrical impedance analysis

The BIA was performed using the IMP SFB7 body composition meter (Impedimed, San Diego, CA). It is a single-channel, tetra-polar bioimpedance spectroscopy device that scans 256 frequencies between 4 and 1000 kHz for the estimation of impedances in tissues. The equipment was calibrated using the calibration cell provided. Needle electrodes (0.5 mm thick and made of stainless steel) were used. A 200 μA RMS AC current flowed through the electrodes. The experimental procedure can be divided into four cases:

Case 1. Five different kinds of fruits and vegetables (apples, eggplants, cucumbers, tomatoes and potatoes) were analyzed. All of them were purchased from a grocery store. Their exact storage time is difficult to determine. Three samples of each kind were tested for ICW content at 22°C. Each sample was cut in the shape of a slab of 2 cm thickness. The electrodes were placed 4 cm apart as shown in Figure 6.

Case 2. Three potato samples (in a slab shape of 2 cm thickness) were placed in an oven (Fisher Isotemp Oven 200 series 230G) with the air temperature at: (a) 45°C; (b) 55°C; (c) 70°C; (d) 90°C. The humidity was not controlled and there was no forced convection inside the oven. The weights of the samples and the resistances, R_0 and R_{inf}, were measured once every hour for 24 hours of drying upon removal from the oven for a short-time ($\sim$2 minutes).

Case 3. Three eggplant samples (in a slab shape of 2 cm thickness) were placed in an oven with the air temperature at: (a) 55°C; (b) 90°C. The weights of the samples and the resistances, R_0 and R_{inf}, were measured once every hour for 24 hours of drying upon removal from the oven for a short time ($\sim$2 minutes).

Case 4. Three potato samples (in a slab shape of 2 cm thickness) were placed in a 2 kW microwave oven (Sharp R-

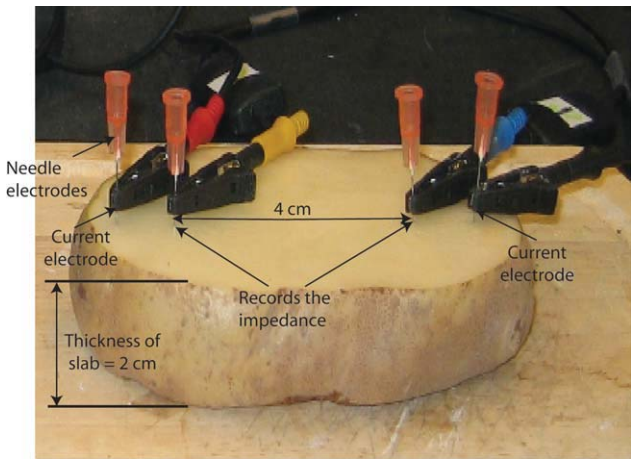

Figure 6. Picture of the experimental setup for bioelectrical impedance analysis.

The needle electrodes are connected to the instrument (not shown in the picture). [Color figure can be viewed in the online issue, which is available at wileyonlinelibrary.com.]

310D(w)C, 120 V, 60 Hz, 1.5 kW). The weights of the samples and the resistances, R_0 and R_{inf}, were measured every 20 seconds of heating upon removal from the microwave oven for a short time (~2 minutes). The total cumulative heating time is 2 minutes.

Results and Discussion

Is the water present in the capillaries (intercellular spaces)?

Both experimental setups for the measurement of capillary pressure, the classical pressure plate experiment and liquid extrusion porosimetry, yielded similar results. Both of them produced little flow even at very high pressures. The pressure plate experiment did not register any water flowing out of the potato for applied pressures between 0.1 and 0.5 MPa, and only 2% of the water flowed out at an applied pressure of 1.5 MPa (the highest possible pressure for this apparatus). The liquid extrusion porosimeter also gave similar results as only 2% of the total water flowed out at an applied pressure of 0.7 MPa (the highest possible pressure for this apparatus). The two different experimental setups, pressure plate and extrusion porosimetry, provide two different approaches to obtaining the pressure-driven flow, and therefore together these results demonstrate that only 2% of total water can be driven out by pressures up to 1.5 MPa.

Of course, we know that raw potato loses water when left in the atmosphere. The potato slices left open to ambient air at atmospheric pressure lost ~80% of their water over 5 days. This contrasts with the low–pressure driven flow for pressures up to 1.5 MPa. The plausible reasons for this can be: (1) the rest of the water is not present in the capillaries; (2) the capillary pressure (which is negative or attractive) is higher than the applied pressure and therefore water cannot flow out of the pores; (3) the water is present in the blind pores (explained in Figure 7), therefore no water flows out, but in that case the moisture migration during drying at atmospheric pressure is not pressure-driven (since pores are not connected). To better understand the pore-sizes and structures, pore-size distribution experiments were performed as described in the next section.

What is the nature of the capillaries?

As explained in the section for the theory behind pore-size distribution, as gas pressure is slowly increased, liquid water is drained out from progressively smaller pores, starting with the largest pores. The flow rate of gas through the dry and wet potato samples at various applied pressures is shown in Figure 8. As can be seen, when drying a wet sample (the wet curve), there is no gas flow initially because the gas cannot displace liquid completely from the pores at this applied pressure. As the pressure is slowly increased on one side of the sample, the gas pressure reaches a point at which it is slightly greater than the surface tension force (or capillary force) of the water and displaces it from the largest pores and thus gas starts to flow out from the other end. As shown in Figure 8, this occurs at around 0.23 MPa. The pore diameter corresponding to this pressure (calculated using Eq. 2) is the largest pore diameter of the sample. For the sample shown in Figure 8, the largest pore diameter is estimated at 0.92 μm and its pore-size distribution is shown in Figure 9. The average pore and smallest pore diameters are 0.53 μm and 0.35 μm, respectively. A total of five samples of potato were tested for pore-size distribution and Table 1 gives the largest and average pore diameter of each of the five samples of the same potato type (Russet white Idaho potatoes). The average over the five samples gives the largest and average pore diameter in this potato type as 3.88 μm and 0.542 μm, respectively. The implications of these are provided in the following paragraph.

Thus, the pore-size distribution study demonstrates that: (1) Pores are not initially empty (since gas does not flow through at low pressures), which leads to two possibilities—either the pores are filled with water (requiring higher pressure) or they are blind pores. (2) Pores are not all blind and there are channels through which water and gas can flow. This is true, since the flow of gas does occur once the liquid is forced out as gas pressure is increased beyond a certain threshold (the bubble point). (3) Pore-sizes larger than 0.35 μm contain only 2% of the total water (that is all the water

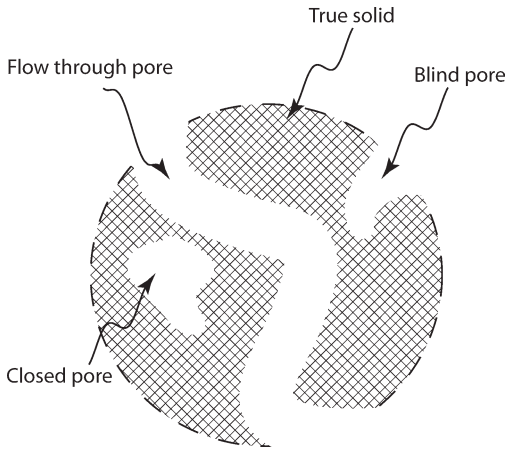

Figure 7. Schematic showing three different types of pores that can be present in a porous material.

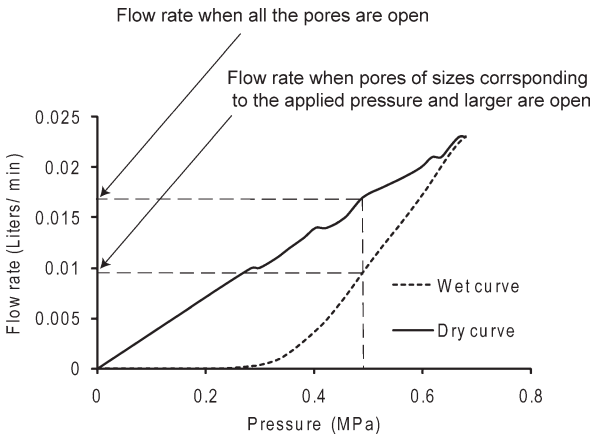

Figure 8. Wet and dry curves obtained during the pore-size distribution experiment of a potato slice.

A wet curve gives the flow rate air at applied pressures when the sample is partially filled with water and the rest consists of empty channels filled with air which allow air to pass. A dry curve gives the flow rate of air at various applied pressures when all the pore channels in the sample are filled with air (pores emptied of water to maximum applied pressure) and allow air to pass through them.

flowing out for pressures up to 0.7 MPa, a pressure that corresponds to a 0.35 μm diameter pore). This leads to the conclusion that either most of the water (98%) is in pores smaller than 0.35 μm in diameter, it is in blind pores, or it is not in pores at all (it is in the cells?). This is discussed in the following section.

If not in the capillaries, is the water present inside cells?

Only a small amount of water can be contained in the intercellular spaces. For example, only 1–2% of the total volume of water occupies intercellular spaces in potato tubers.[39] Therefore, it is unlikely that there is a significant amount of water remaining in the intercellular spaces that can be drained out by applying still higher external pressures. So, the question is, where is the water if it is not in the pores (intercellular spaces)? The biology literature states that at least 70% of the water is intracellular in meat[40] and vegetables[41,42] at room temperature. ICW flow would require cell membranes to rupture at high-pressure (a value of 3 MPa for the rupture of cell walls and cell membranes in carrots was reported by Carpita[43]) that is above the values used for capillary pressure measurements. It appears critical to quantify the amount of ICW, which we accomplished using BIA on potatoes and eggplants, as described in the next section.

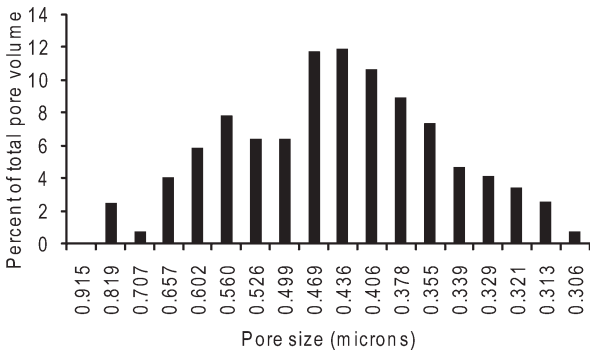

Figure 9. Pore-size distribution of a potato slice.

Largest pore diameter measured was 0.915 μm and smallest was 0.306 μm. Average pore diameter for the slice is 0.499 μm.

Table 1. Summary of Pore-Size Distribution Experiment of Five Potato Samples

Sample Number	Largest Pore Diameter (μm)	Average Pore Diameter (μm)
1	5.736	0.389
2	0.915	0.440
3	5.761	0.554
4	1.267	0.875
5	5.745	0.453
Average	3.885	0.542

How much water is intracellular?

Using BIA, ICW content at room temperature was measured for five different vegetables, as shown in Table 2. Potatoes and eggplants have high ICW at around 95% and tomatoes have relatively lower ICW at around 80%. The experimental results reported in Table 2 closely match the data on ICW content in the literature as measured using other experimental procedures, such as freezing.[42]

As potato has around 95% ICW at room temperature, only 5% of the water in the pores would be forced out by applied pressure (in the range discussed in first paragraph under Is the water present in the capillaries (inter cellular spaces)?). This is consistent with what occurred during the capillary pressure measurement and pore-size distribution experiments, where 2% of the water could be driven out on the application of pressure at 0.7 MPa.

Figure 10 shows the Cole–Cole plot for a sample measured at different times while drying at 90°C. The resistance at zero frequency, R_0, which is inversely proportional to extracellular water content, decreases with an increase in temperature. The value of R_0 for a raw potato is 2300 ohms, which decreases to 1100 ohms after 30 minutes and 150 ohms after 105 minutes of drying. A decrease in R_0 means an increase in extracellular water content and this can be explained if cell membranes are damaged and ICW is released into the matrix.

That cell membrane damage releases water into the extracellular matrix is further illustrated in Figure 11 which shows the variation with the temperature in resistance and reactance of the sample at the same signal frequency. From this figure, the temperature range in which the cells get damaged and release water in the matrix can be estimated. As the temperature increases from 20 to 50°C, the resistance decreases slightly with the temperature due to an increase in conductance of the fluids. Similar observations were also made during BIA of skin.[44] The capacitance of the cell increases with the temperature[45] and this should lead to a decrease in reactance, as also shown in Figure 11. Between 52 and 60°C, there is a sharp drop in resistance and reactance. Resistance decreases suddenly because, as the cell membrane ruptures, the cross-sectional area through which

Table 2. Intracellular Water Content (%) of Different Cellular Products at Room Temperature (22°C), Measured Using Bioimpedance Analysis Technique

Sample	Intracellular Water Content (%)
Cucumber (Sample 1)	95.3
Cucumber (Sample 2)	95.8
Tomato (Sample 1)	84.7
Tomato (Sample 2)	78.7
Apple (Sample 1)	90.2
Apple (Sample 2)	89.9
Eggplant (Sample 1)	96.8
Eggplant (Sample 2)	97.3
Potato (Sample 1)	95.3
Potato (Sample 2)	96.0

the current is passing increases significantly, thus reducing the resistance (resistance is inversely proportional to cross-sectional area). The above reasoning is based on the assumption that the cell rupture does not result in a change in extracellular resistivity. The damage to the cell also causes a reduction in the potential across the membrane produced by the applied current, thus reducing the current flowing into the membrane capacitance.

BIA in low-temperature drying The potato samples were dried in an oven for 24 hours at two temperatures (45°C and 55°C) to estimate the range of temperatures within which the cell damage takes place and the ICW is released into the intercellular space. Figures 12a, b give the variations in moisture content (kg water /kg dry weight), temperature and the percentage of ICW content (ICW) of potato slice while drying at 45°C. In Figure 12a, it can be seen that, during the drying process, the potato samples lose water significantly (moisture content dropped from 4.35 to 2.75). Figure 12b shows that the temperature inside the potato always remains below 42°C and ICW remains stable at around 96% throughout the drying process. This means that the cells lose water to the outside during the process but they are not damaged

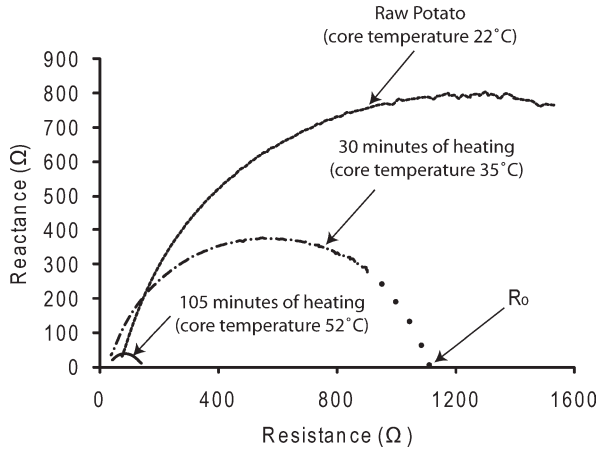

Figure 10. Cole–Cole plot for a potato slice, heated at 90°C, is obtained from BIA.

The semi-circular nature of the plot allows the determination of R_{inf} and R_0 by extrapolation to touch the horizontal axis. As temperature increases inside the potato (with drying time), R_0 decreases, signifying increased pathways through the extracellular water (thus increased amount of extracellular water).

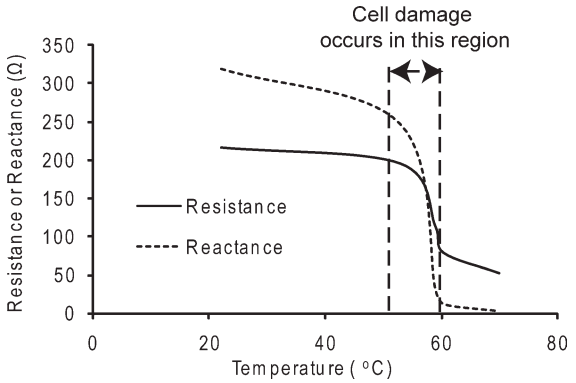

Figure 11. Variation of resistance and reactance with temperature at 50 kHz.

The temperature range where resistance and reactance drops sharply (between 52 and 60°C) is identified as the range where the cell membranes get damaged.

and the cell membranes remain intact throughout. So, the water migration pathway during this process can be called an intracellular pathway, as shown in Figure 17a, where water migrates through three different zones in series: cell membranes, cell walls and intercellular spaces.

During the drying of potato slices at 55°C (shown in Figures 12c, d), the ICW remains stable at 96% until the temperature nears 50°C (300 minutes of drying). As the temperature rises above 50°C, the ICW drops slowly and reaches 60% after 24 hours of drying. Based on these results it can be said that the cell membrane remains intact until the temperature reaches about 50°C and is ruptured as the temperature rises above that temperature, thereby releasing water into the intercellular space and increasing the fraction of extracellular water. The sample loses water significantly during this higher temperature period (shown in Figure 12c). The water migration during the initial period of drying (in the first 300 minutes when the cells are intact) would proceed through the intracellular pathways (just as when drying the slices at 45°C). When the cell membrane ruptures, the released water travels through intercellular space and this is called an extracellular pathway (shown in Figure 17b). In an extracellular pathway, the migrating water experiences no resistance from cell membranes. Thus, when drying potato slices at 55°C, during the initial period the moisture migrates primarily through intracellular pathways. During the later stages, when the cell membranes rupture, some of the water migrates through extracellular pathways but the movement is still primarily intracellular as ICW remains above 60%.

Similar observations were also made from the low-temperature drying experiments with eggplant (e.g., eggplant dried at 55°C). As can be seen in Figure 13, the ICW remains constant at around 97% until the temperature reaches about 50°C and then decreases slowly to 75% at the end of 24 hours of drying (during which time the temperature remains above 50°C). In Figure 13a, it can be seen that the eggplant loses a significant amount of water (moisture content dropped from 15.9 to 5.01) during this period. The moisture migration in eggplant during drying at 55°C is similar to what occurs in potato drying at 55°C: moisture migrates

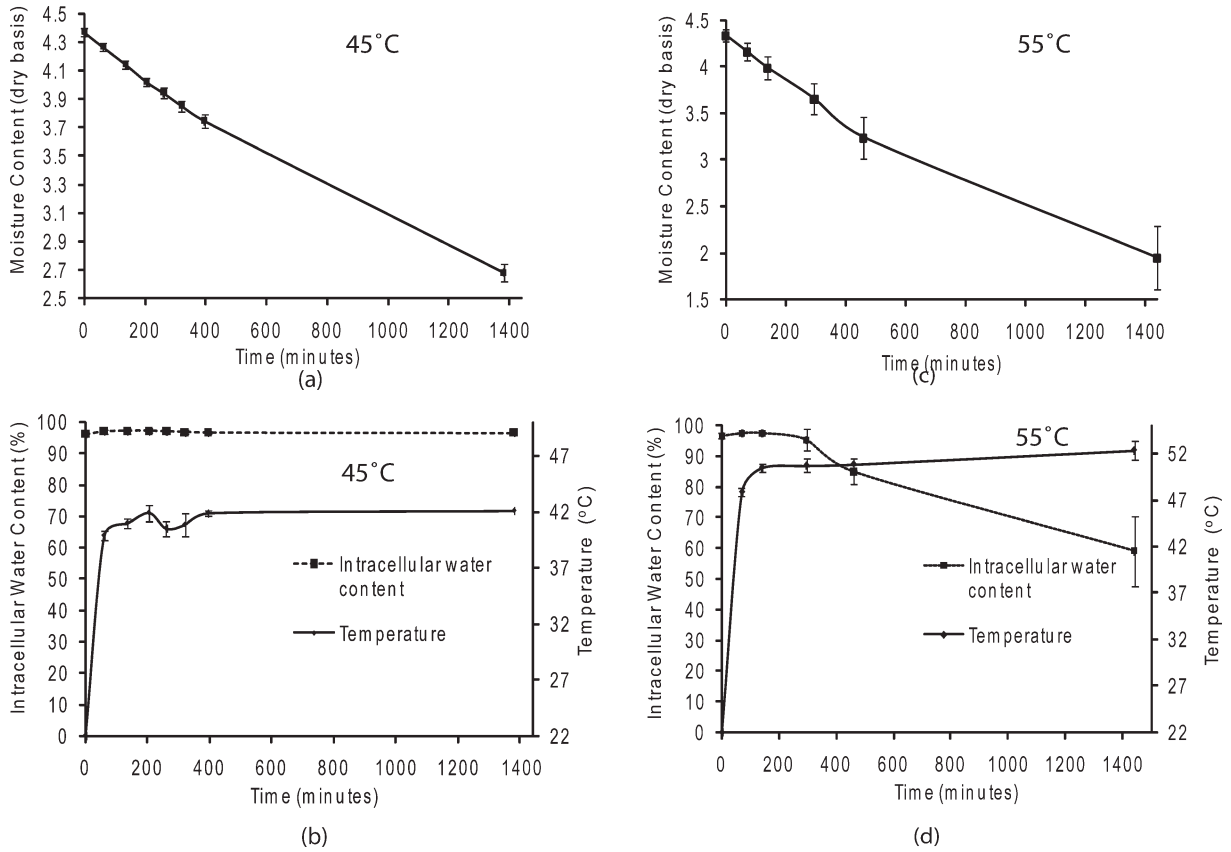

Figure 12. Moisture content (kg water/ kg dry weight) versus time for drying of potato slice at (a) 45°C and (c) 55°C.

Intracellular water content (%) and core temperature versus time for drying of potato slice at (b) 45°C and (d) 55°C.

almost exclusively along intracellular pathways in the initial stages, followed by both intracellular and extracellular pathways, although 75% of the water migration is still intracellular.

BIA in high-temperature drying Potato and eggplant slices were dried at high temperatures and their ICW values were measured at regular time intervals to see how higher temperatures affect ICW. The potato samples were dried and analyzed at two temperatures (70°C and 90°C), the results of which are shown in Figure 14. The ICW starts decreasing as soon as the core temperature rises above 50°C. But in the case of high-temperature drying, the time required to reach 50°C is short and the sample is under the effect of high temperatures for a longer period of time and therefore shows lower ICW after 24 hours of drying. Water migration primarily follows extracellular pathways during high-temperature drying. As in the case of drying at 90°C (shown in Figure 14d), after 200 minutes there is no ICW. In the case of drying at 70°C, the migration primarily follows intracellular pathways initially (until 100 minutes) but primarily extracellular pathways in the last 300 minutes. In between, the migration involves both intracellular and extracellular pathways. Similar results were observed in the case of drying eggplant at 90°C (shown in Figure 15).

BIA in microwave heating of potatoes Microwaves heat more rapidly and possibly more uniformly, which should lead to differences in ICW during the heating process. In microwave heating of a potato sample, ICW remained constant while the temperatures were below 62°C and then declined sharply to 40% after 2 minutes of heating (as shown in Figure 16b). Microwave heating is rapid and cell membranes at high temperatures do not rupture instantaneously. Therefore, by the time most cell membranes rupture inside the potato, the sample temperature rises to 62°C. This explains why evidence of cell membrane rupture is observed at higher temperature than when drying. As shown in Figure 16a, moisture content does not change much during the 2 minutes of microwave heating, and the ICW drops to 40%. Therefore, initially (in the first 2 minutes) the moisture migration proceeds through both intracellular and extracellular pathways but the amount of water lost during this time is less than 5%. In the later stages of microwave heating (after 2 minutes and not shown in the figure), when most of the moisture loss takes place, the cell membranes are damaged and the water is released into the matrix, leading to an extracellular pathway. Note that, at a temperature of 62°C, pressure generated due to evaporation from microwave heating is unlikely to have any significant effect on cell membrane rupture.

A summary of where the water is

Based on the porosimetry and bioimpedance analyses, it can be concluded that most of the water is not in the pores

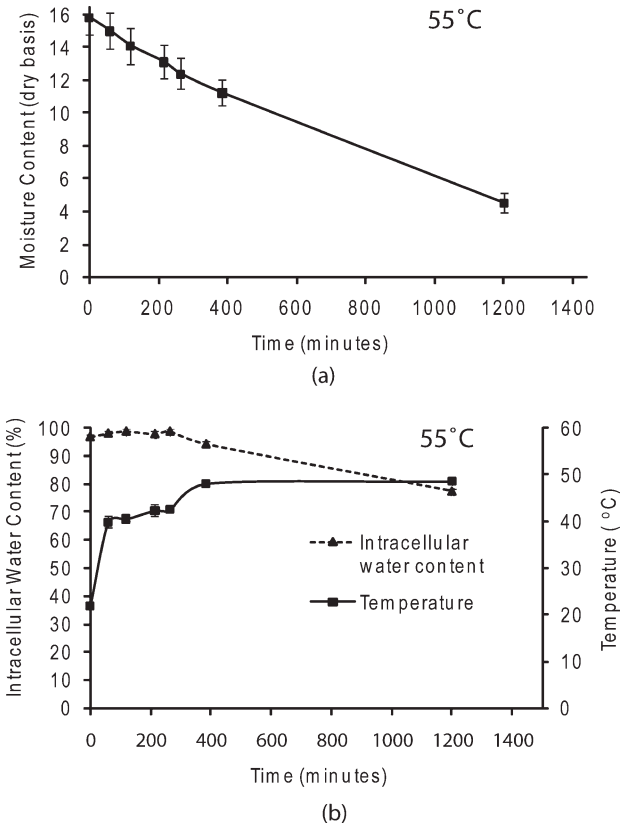

Figure 13. (a) Moisture content (kg water/ kg dry weight) and (b) Intracellular water content (%) and core temperature versus time for drying of eggplant slice at 55°C.

but in the cells. In fact, more than 90% of the water inside the potato tissue is intracellular at 22°C. At temperatures in the range of 52–60°C, the cell membranes rupture (ICW content decreases drastically) and water is released into the extracellular matrix. This conclusion is consistent with our porosimetry measurements where flow did not occur at the lower temperatures for very high pressures. In carrots, for example, the pressure required to rupture cell walls and cell membranes is 3 MPa[43] and the pressures used (0.7 MPa) in our capillary pressure and pore-size distribution measurements were not sufficient to rupture the cell walls and cell membranes and drive out the ICW. Although one obvious possibility is to repeat the pressure-driven flow experiments for potatoes at higher temperatures, the available instrument does not permit this measurement due to the softness of the potato at higher temperatures. In the next two sections, we discuss the implications of the location of water on its transport.

Water transport at low temperatures: cell membrane is intact

The main source of water in a tissue is the cell. As shown in the experiments with BIA, more than 90% of the water inside potato tissue is intracellular at 22°C. At low temperatures (between 22 and 50°C), the cell membranes remain intact and the transport of water out of the tissue involves migration through both the cells and extracellular space. The main pathway, as shown in Figure 17a, can be described in terms of water moving from inside the cells through the cell membranes and then the cell walls into the intercellular space. This moisture transport takes place due to the gradient of water potential between cells and the intercellular spaces. The migrating moisture meets resistance from the cell membranes, cell walls and the intercellular spaces—whichever offers maximum resistance controls the transport.

Next, we compute the flux of water from inside the cell to the outside. The water potential (the driving force for water transport) inside and outside the cell can be expressed as

$$\begin{aligned}\phi_{\mathrm{w,intra}} &= \phi_{\mathrm{w},0} + R_{\mathrm{g}}T\ln(a_{\mathrm{w,intra}})\\ \phi_{\mathrm{w,extra}} &= \phi_{\mathrm{w},0} + R_{\mathrm{g}}T\ln(a_{\mathrm{w,extra}})\end{aligned} \tag{15}$$

Therefore, the water potential difference driving the flow of water from inside the cell to outside is given by

$$\Delta\phi_{\mathrm{w}} = R_{\mathrm{g}}T\ln(a_{\mathrm{w,intra}}) - R_{\mathrm{g}}T\ln(a_{\mathrm{w,extra}}) \tag{16}$$

The relationship of water activity, a_{w}, to moisture content at constant temperature is known as a moisture isotherm and is readily available for many different food materials. The difference in pressure due to the water potential difference can be expressed as[8]

$$\Delta p_{\mathrm{w}} = \frac{R_{\mathrm{g}}T}{V_{\mathrm{w}}}\ln(a_{\mathrm{w,intra}}) - \frac{R_{\mathrm{g}}T}{V_{\mathrm{w}}}\ln(a_{\mathrm{w,extra}}) \tag{17}$$

where p_{w} is referred to as capillary pressure in the food literature but is essentially the lumped effect of all the surface forces acting on the fluid. Assuming Darcy's flow, the water flux through the tissue can be written as

$$J_{\mathrm{w}} = -\rho_{\mathrm{w}}\frac{k_{\mathrm{eff}}}{\mu_{\mathrm{w}}}\frac{\Delta p_{\mathrm{w}}}{\Delta x} \tag{18}$$

where k_{eff} is the effective permeability through the tissue (a lumped parameter including the effect of transport through cell walls, cell membranes, and intercellular spaces). Equation 18 is analogous to the water flux equation, $J_{\mathrm{w}} = \rho_{\mathrm{w}}L_{\mathrm{w}}(\Delta p_{\mathrm{w}})$, commonly used in the plant physiology field. The relationship between hydraulic conductivity (L_w used in plant physiology literature) and permeability (k used in this manuscript) can be written as

$$L_{\mathrm{w}} = \frac{k_{\mathrm{eff}}}{\mu_{\mathrm{w}}\Delta x} \tag{19}$$

Next, we compute the individual permeabilities ($L_{\mathrm{w}}\mu_{\mathrm{w}}t$ or k) offered by cell walls, cell membranes and intercellular spaces to migrating moisture. The literature has recorded only a small amount of permeability (k) data for water through various biological tissues, cell walls, and cell membranes. In tissues, permeability is reported to be on the order of 10^{-18} m^2 for potato and beef[15] and in the range of 10^{-18} m^2 to 10^{-16} m^2 for ground beef.[16] Based on our interpretation of the measurement techniques used in these studies, we strongly feel that these data (for potato and beef) represent permeability through the largest of the pores in the

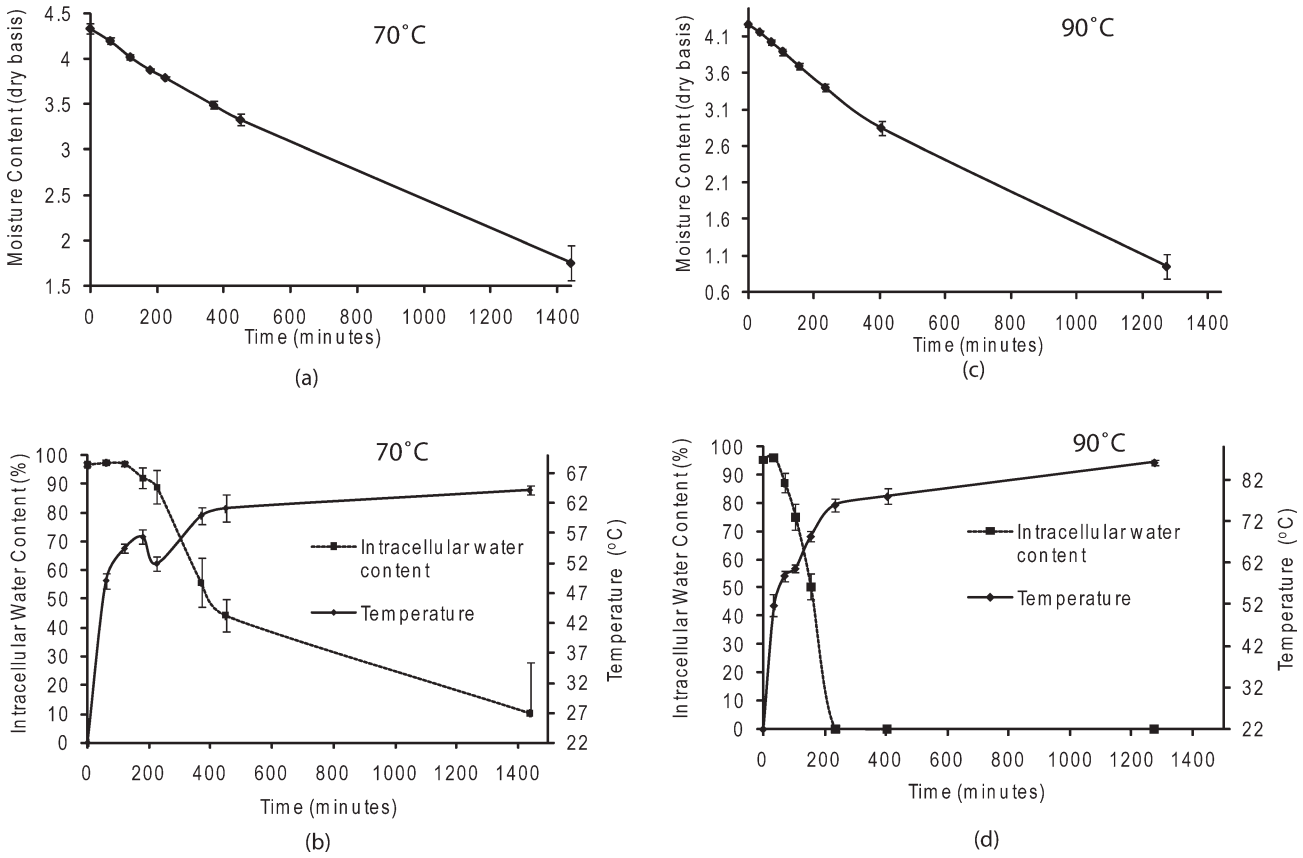

Figure 14. Moisture content (kg water/ kg dry weight) versus time for drying of potato slice at (a) 70°C and (c) 90°C.

Intracellular water content (%) and core temperature versus time for drying of potato slice at (b) 70°C and (d) 90°C.

intercellular space. For cell walls, permeability in fruits and vegetables is not available but permeability of water through cell walls of spruce heartwoods was found to be between 4.03×10^{-21} m^2 and 67.5×10^{-21} m^2,[46] which can be representative of the values in fruits and vegetables because both are plant cells and the cell walls exhibit similar structure. The value of 5×10^{-20} m^2 found for *Nitella* (a plant) cell walls (converted from $L_w = 30$ μm min^{-1} atm^{-1} in[47] using Eq. 19 and thickness of cell wall as 10^{-5} m) is in the same range observed by Palin and Petty[46] for spruce heartwoods. For cell membranes, the permeability for potato cells has been reported as 10^{-24} m^2 (converted from $L_w = 10^{-13}$ m s^{-1} Pa^{-1} in[48] using Eq. 19 and thickness of cell membrane as 10^{-8} m). Because the cell membrane exhibits three orders of magnitude lower permeability, it is likely to be the controlling resistance to transport at lower-temperatures.

In continuum mechanics treatment of flow in an unsaturated porous media, flux given by Eq. 18 is rewritten in terms of a concentration gradient as (see, e.g., Ref. 33)

$$J_w = -\rho_w \frac{k_{eff}}{\mu_w} \frac{\Delta p_w}{\Delta c_w} \frac{\Delta c_w}{\Delta x} = -D_w \nabla c_w \tag{20}$$

where D_w is the capillary diffusivity (not molecular diffusivity) of water through the cell membrane and, from Eq. 20, it can be written as

$$D_w = \rho_w \frac{k_{eff}}{\mu_w} \frac{\Delta p_w}{\Delta c_w} = \rho_w \frac{k_{eff}}{\mu_w} \frac{\partial p_w}{\partial c_w} \tag{21}$$

In practice, D_w is treated as an effective diffusivity, that includes all transport mechanisms, including capillarity. Equation 21 shows that D_w depends on the permeability. Based on the discussion in the previous paragraph, that cell membrane permeability is the controlling resistance for low-temperature drying (since the cell membranes are not ruptured at lower-temperatures), the relevant permeability in moisture diffusivity, D_w, is the cell membrane permeability. Using the moisture isotherm data for potato tissue[49] and the cell membrane permeability of potato tissue[48] of 10^{-21}m^2, the diffusivity is computed (using Eq. 21) to be on the order of 10^{-11}m^2/s. Experimentally measured diffusivity of water through potatoes is on the order of 10^{-11}m^2/s for air drying at 30°C,[50] showing the same order of magnitude as our predicted results. At this temperature, cell membranes are intact and the diffusivity value obtained corresponds to the intracellular pathway.

Water transport at high temperatures: cell membrane is destroyed

At high temperatures, cell membranes rupture and release water into the extracellular space (schematic in Figure 17b) and therefore the transport of water to the outside occurs

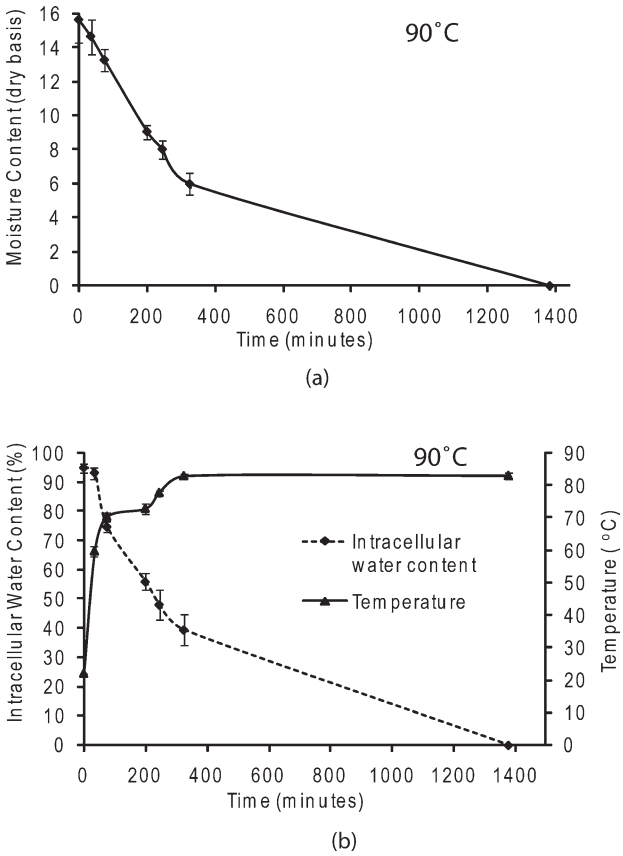

Figure 15. (a) Moisture content (kg water/ kg dry weight) and (b) Intracellular water content (%) and core temperature versus time for drying of eggplant slice at 90°C.

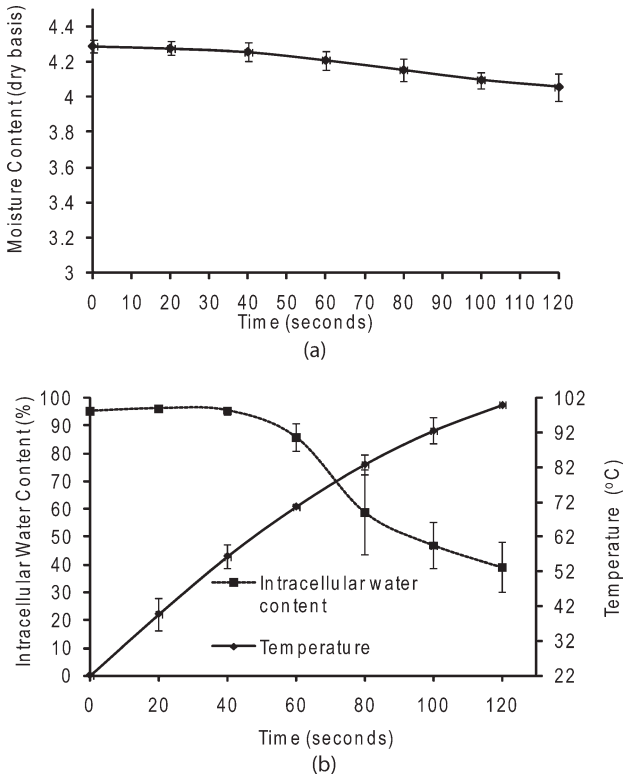

Figure 16. (a) Moisture content (kg water/ kg dry weight) and (b) Intracellular water content (%) and core temperature versus time for drying of potato slice during microwave heating.

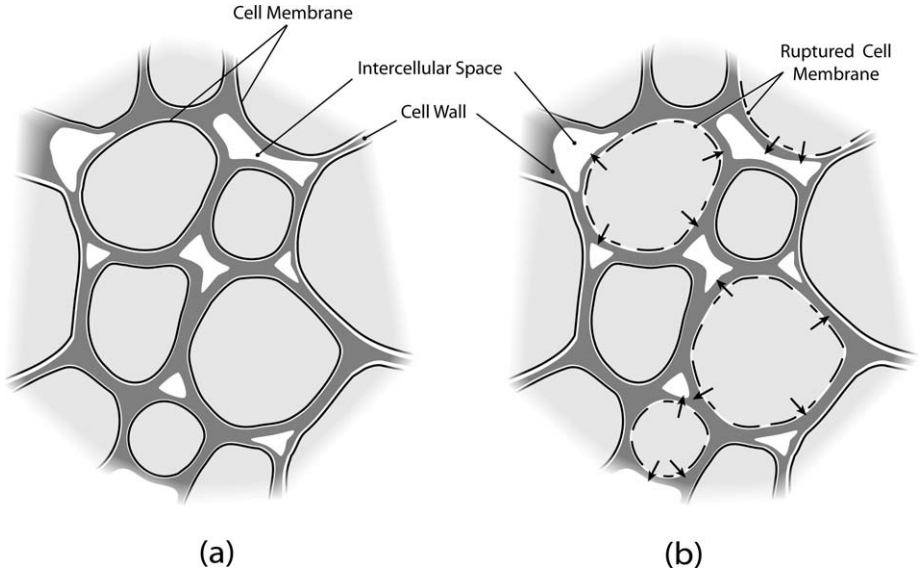

Figure 17. Schematic showing the cell membrane structure at (a) temperatures below 52°C (low temperatures); (b) temperatures above 52°C (high temperatures).

At low temperatures, the moisture migration faces resistance from cell membranes, cell walls and intercellular spaces. At high temperatures, the cell membrane is ruptured. The moisture migration faces resistance from cell walls and intercellular spaces.

predominantly through the extracellular space. Applying Darcy's law in the intercellular space, the water flux can be written as

$$J_w = -\rho_w \frac{k_{out}}{\mu_w} \frac{\Delta p_w}{\Delta x} \tag{22}$$

Therefore, similar to Eq. 21, D_w for migration at high temperatures can be written as

$$D_w = -\rho_w \frac{k_{out}}{\mu_w} \frac{\partial p_w}{\partial c_w} \tag{23}$$

The main difference between the diffusivity value at high temperature and that at low temperature is found in the corresponding permeability values. For high temperature, the permeability is that of intercellular spaces, approximated from literature studies as $10^{-18}m^2$ (see discussion in the previous section), in contrast with the much lower value of $10^{-24}m^2$ for low temperatures discussed in the previous section, where it is attributed to permeability of cell membranes. The diffusivity calculated for a permeability of $10^{-18}m^2$ is on the order of $10^{-7}m^2/s$. The water diffusivity in potato tissues has been reported as $10^{-9}m^2/s$ during drying at 70°C.[51] At this temperature, around 20–30% of water may still be intracellular (as shown in Figure 14b), which explains the reduced diffusivity value observed in the experiments. Drying at 70°C is in the mid range and perhaps explains the diffusivity of $10^{-9}m^2/s$ between the two extremes.

Conclusions

Transport of water in a cellular tissue was studied using potatoes. Based on the experimental results, it is concluded that transport of water depends on its pathway (intracellular versus extracellular), which in turn depends on temperature. Using a combination of permeability measurement, pore-size distribution analysis and bioimpedance analysis, it is shown that water in a cellular tissue is mostly intracellular at lower-temperatures when cell membranes are intact. This explains why very little water (~2%) can be pushed out by applying pressures up to 1.5 MPa. Using BIA, it was observed that ~95% of the water is intracellular in potato tissue at lower temperatures, and this water becomes extracellular at temperatures above 52°C when the cell membranes rupture. Also, data in the literature shows that cell membrane permeabilities are at least three orders of magnitude lower than those in the cell walls and other extracellular space. Therefore, when drying at lower-temperatures, cell membranes are not damaged, the pathway of moisture transport is intracellular, and resistance to transport is dominated by cell membranes—resulting in a lower moisture diffusivity value. During drying at high temperatures, cell membranes are damaged and the moisture transport pathway is primarily extracellular (through intercellular space and the lacunae created by dead cells), which offers lower resistance, leading to a higher moisture diffusivity value. The difference in diffusivity for the two pathways has been estimated to be three orders of magnitude, consistent with experimental data reported in the literature. Thus, transport properties measured or predicted at low temperatures cannot be used for high temperatures because the processes correspond to different moisture migration pathways.

Acknowledgments

This research was partially supported by the United States Department of Agriculture Regional Project NC 1023 and the United States Department of Agriculture National Integrated Food Safety Project 2004-51110-02167. The authors thank Prof. Apostolos Kantzas in Chemical and Petroleum Engineering Department, University of Calgary, and Dr. Akshaya Jena in Porous Materials Inc., Ithaca, for assistance with the discussion of capillary pressure measurement techniques. They also thank Josh Powers and Terry Murray in Porous Materials Inc., Ithaca, and Robert Schindelbeck in Crop and Soil Sciences, Cornell University, for all their help during the experiments.

Notation

a = water activity
c = concentration (kg m^{-3})
C = capacitance (Farad)
d = diameter of pore (m)
D = diffusivity (m^2 s^{-1})
F = flow rate (m^3 s^{-1})
f = frequency of signal (Hz)
J = flux (kg m^{-2} s^{-1})
k = permeability (m^2)
L = length of the channel (m)
M = moisture content (dry weight basis) (kg water / kg dry weight)
N = total number of pores
n = number of pores
p = pressure (Pa)
R = resistance (ohms)
R_g = universal gas constant
t = thickness of cell membrane (m)
V = volume (m^3)
X = reactance (ohms)
Z = impedance (ohms)

Greek letters

β = electrical resistivity (Ohm m)
γ = surface tension (N m^{-1})
κ = ratio of electrical resistivity
μ = viscosity (Pa s)
ω = angular frequency (Hz)
ϕ = chemical potential (J mol^{-1})
ρ = density (kg m^{-3})
θ = contact angle between liquid water and surface

Subscripts

a = air
e = extracellular
eff = effective
i = intracellular
w = water
0 = zero frequency
cap = capillary
ECW = extracellular water
ICW = intracellular water
inf = infinite frequency

Literature Cited

1. Ateba P, Mittal GS. Modeling the deep-fat frying of beef meatballs. *Int. J. Food Sci. Technol.* 1994;29:429–440.
2. Ikediala JN, Correia LR, Fenton GA, BenAbdallah N. Finite element modeling of heat transfer in meat patties during single-sided pan-frying. *J. Food Sci.* 1996;61:796–802.
3. King CJ. Rates of moisture sorption and desorption in porous, dried foodstuffs. *Food Technol.* 1968;22:165–171.

4. Rotstein E. The prediction of diffusivities and diffusion-related transport properties in the drying of cellular foods. *Phys. Properties Foods* 1987;2:131–145.
5. Ni H, Datta AK. Moisture, oil and energy transport during deep-fat frying of food materials. *Food Bioproducts Process.* 1999;77: 194–204.
6. Yamsaengsung R, Moreira RG. Modeling the transport phenomena and structural changes during deep fat frying — Part 1: model development. 2002. *J. Food Eng.* 2002;53:1–10.
7. Halder A, Dhall A, Datta AK. An improved, easily implementable, porous media based model for deep-fat frying — Part I: Model development and input parameters. *Food Bioproducts Process.* 2007;85:209–219.
8. Gee GW, Campbell MD, Campbell GS and Campbell JH. Rapid measurement of low soil water potentials using a water activity meter. *Soil Sci. Soc. Am. J.* 1992;56:1068–1070.
9. Conca JL, Wright J. The UFA method for rapid, direct measurements of unsaturated transport properties in soil, sediment, and rock. *Aust. J. Soil Res.* 1998;36:291–315.
10. Khanzode RM, Vanapalli SK, Fredlund DG. Measurement of soil-water characteristic curves for fine-grained soils using a small-scale centrifuge. *Can. Geotech. J.* 2002;39:1209–1217.
11. Hassler GL, Brunner E. Measurement of capillary pressures in small core samples. *Trans. Am. Inst. Min. Metall. Eng.* 1945;160:114–123.
12. Reitsma S, Kueper BH. Laboratory measurement of capillary-pressure saturation relationships in a rock fracture. *Water Res. Res.* 1994;30:865–878.
13. Chen ZA, Ruth DW. Ramp-up centrifugation of capillary pressure experiments. *AIChE J.* 1997;43:2133–2136.
14. Spolek GA, Plumb OA. Capillary pressure in softwoods. *Wood Sci. Technol.* 1981;15:189–199.
15. Datta AK. Hydraulic permeability of food tissues. *Int. J. Food Properties.* 2006;9:767–780.
16. Oroszvari BK, Rocha CS, Sjoholm I, Tornberg E. Permeability and mass transfer as a function of the cooking temperature during the freezing of beefburgers. *J. Food Eng.* 2006;74:1–12.
17. Farkas BE, Singh RP. Physical-properties of air-dried and freeze-dried chicken white meat. *J. Food Sci.* 1991;56:611–615.
18. Kassama LS, Ngadi MO. Pore development in chicken meat during deep-fat frying. *Lebensm-Wiss. Technol.* 2004;37:841–847.
19. Datta AK, Sahin S, Sumnu G, Keshin SO. Porous media characterization of breads baked using novel heating modes. *J. Food Eng.* 2007;79:106–116.
20. Lukaski HC, Johnson PE, Bolonchuk WW, Lykken GL. Assessment of fat-free mass using bioelectrical impedance measurements of the human body. *J. Clin. Nutr.* 1985;41:810–817.
21. Matthie JR, Withers PO, Van Loan MD, Mayclin PL. Development of a commercial complex bio-impedance spectroscopic (CBIS) system for determining intracellular water (ICW) and extracellular (ECW) volumes. In: Proceedings of the 8th International Conference on Electrical Bio-impedance Kuopio Finland 1992, Kuopio, Finland, University of Kuopio, 1992:203–205.
22. Zhang MIN, Stout DG, Willison JHM. Electrical-impedance analysis in plant-tissues - symplasmic resistance and membrane capacitance in the Hayden model. *J. Exp. Botany.* 1990;41:371–380.
23. Cox MA, Zhang MIN, Willison JHM. Apple bruise assessment through electrical-impedance measurements. *J. Hortic. Sci.* 1993;68: 393–398.
24. Harker FR, Dunlop J. Electrical impedance studies of nectarines during coolstorage and fruit ripening. *Postharvest Biol. Technol.* 1994;4:125–134.
25. Dejmek P, Miyawaki O. Relationship between the electrical and rheological properties of potato tuber tissue after various forms of processing. *Biosci. Biotechnol. Biochem.* 2002;66:1218–1223.
26. Wu L, Ogawa Y, Tagawa A. Electrical impedance spectroscopy analysis of eggplant pulp and effects of drying and freezing-thawing treatments on its impedance characteristics. *J. Food Eng.* 2008;87: 274–280.
27. Hills BP, Nott KP. NMR studies of water compartmentation in carrot parenchyma tissue during drying and freezing. *Appl. Magn. Reson.* 1999;17:521–535.
28. Hills BP, Remigereau B. NMR studies of changes in subcellular water compartmentation in parenchyma apple tissue during drying and freezing. *Int. J. Food Sci. Technol.* 1997;32:51–61.
29. Hills BP, Floc'h GL. NMR studies of non-freezing water in cellular plant tissue. *Food Chem.* 1994;51:331–336.
30. Prothon F, Ahrne L, Sjoholm I. Mechanisms and prevention of plant tissue collapse during dehydration: a critical review. *Crit. Rev. Food Sci. Nutr.* 2003;43:447–479.
31. Hassanizadeh SM, Gray WG. Thermodynamic basis of capillary pressure in porous media. *Water Resources Res.* 1993;29:3389–3405.
32. Gardener WR. Calculation of capillary conductivity from pressure plate outflow data. *Soil Sci. Soc. Am. Proc.* 1956;20:317–320.
33. Bear J. *Dynamics of Fluids in Porous Media*. New York: American Elsevier Publishing Company, 1972.
34. Gupta N, Jena A. Determining the pore structure of individual layers of multi-layered ceramic composites. *Ceram. Ind.* 2001;151:24–29.
35. Cole KS. *Membranes, Ions and Impulses: A Chapter of Classical Biophysics*. Los Angeles: UCLA press, 1972.
36. Hanai T. *Electrical properties of emulsions*. In: Sherman PH, editor. *Emulsion Science*. London: Academic press. 1968:354–477.
37. De Lorenzo A, Andreoli A, Matthie J, Withers P. Predicting body cell mass with bioimpedance by using theoretical methods: a technological review. *J. Appl. Physiol.* 1997;82:1542–1548.
38. Dainty J, Hope AB. The electric double layer and the Donnan equilibrium in relation to plant cell walls. *Aust. J. Plant Physiol.* 1961;14:541–551.
39. Hudson DE. Relationship of cell-size, intercellular space, and specific gravity to bruise depth in potatoes. *Am. Potato J.* 1975;52:9–14.
40. Honikel KO, Hamm R. *Measurement of Water-Holding Capacity and Juiciness, Quality Attributes in Meat, Poultry and Fish Products*. London: Blackie Academic and Professional Publication, 1994:125–161.
41. Nobel PS. *Cells and Diffusion, Physicochemical and Environmental Plant Physiology*, 4th ed. San Diego, CA: Elsevier, Inc., 2009:3–42.
42. Asquith MH, Kirk E, Kirkland M, Morrey SM, Ormerod AP, Ralfs JD, Sharp DG, Sidebottom CM. Freezing vegetables. US Patent 7,169,426. January 30, 2007.
43. Carpita NC. Tensile strength of cell walls of living cells. *Plant Physio.* 1985;79:485–488.
44. Cornish BH, Thomas BJ, Ward LC. Effect of temperature and sweating on bioimpedance measurements. *Appl. Radiat. Isotopes.* 1998;49:475–476.
45. Leuchtag HR. Fit of the dielectric anomaly of squid axon membrane near heat-block temperature to the ferroelectric Curie-Weiss law. *Biophys. Chem.* 1995;53:197–205.
46. Palin MA, Petty JA. Permeability to water of the wood cell wall and its variation with temperature. *Wood Sci. Technol.* 1983;17:187–193.
47. Kamiya N, Tazawa M, Takata T. Water permeability of the cell wall in Nitella. *Plant Cell Physiol.* 1962;3:285–292.
48. Rotstein E, Cornish ARH. Influence of cellular membrane permeability on drying behavior. *J. Food Sci.* 1978;43:926–939.
49. Ratti C, Crapiste GH, Rotstein E. A new water sorption equilibrium expression for solid foods based on thermodynamic considerations. *J. Food Sci.* 1989;54:738–742.
50. Saravacos GD. Effect of drying method on the water sorption of dehydrated apple and potato. *J. Food Sci.* 1967;32:81–84.
51. Mulet A. Drying modeling and water diffusivity in carrots and potatoes. *J. Food Eng.* 1994;22:329–348.

Manuscript received Jan. 5, 2010, revision received Aug. 26, 2010, and final revision received Oct. 5, 2010.